



# High purity $^{47}\text{Sc}$ production using high-energy photons and natural vanadium targets

December 2021

*Changing the World's Energy Future*

Mathew S Snow, Ariana A Foley, Jessica L Ward, Hayden P Town, Kevin P Carney, Mathew Kinlaw



**DISCLAIMER**

This information was prepared as an account of work sponsored by an agency of the U.S. Government. Neither the U.S. Government nor any agency thereof, nor any of their employees, makes any warranty, expressed or implied, or assumes any legal liability or responsibility for the accuracy, completeness, or usefulness, of any information, apparatus, product, or process disclosed, or represents that its use would not infringe privately owned rights. References herein to any specific commercial product, process, or service by trade name, trade mark, manufacturer, or otherwise, does not necessarily constitute or imply its endorsement, recommendation, or favoring by the U.S. Government or any agency thereof. The views and opinions of authors expressed herein do not necessarily state or reflect those of the U.S. Government or any agency thereof.

# **High purity $^{47}\text{Sc}$ production using high-energy photons and natural vanadium targets**

**Mathew S Snow, Ariana A Foley, Jessica L Ward, Hayden P Town, Kevin P Carney, Mathew Kinlaw**

**December 2021**

**Idaho National Laboratory  
Idaho Falls, Idaho 83415**

**<http://www.inl.gov>**

**Prepared for the  
U.S. Department of Energy  
Under DOE Idaho Operations Office  
Contract DE-AC07-05ID14517**

1 High Purity  $^{47}\text{Sc}$  Production Using High-Energy  
2 Photons and Natural Vanadium Targets

3 *Mathew S. Snow\*<sup>1</sup>, Ari Foley<sup>1</sup>, Jessica L. Ward<sup>1</sup>, Mathew T. Kinlaw<sup>1</sup>, Jon Stoner<sup>2</sup>, Kevin P.*  
4 *Carney<sup>1</sup>*

5  
6 1-Idaho National Laboratory, PO Box 1625, Idaho Falls, ID 83415-2805, USA

7 2- Idaho Accelerator Center, 1500 Alvin Ricken Drive, Pocatello, ID 83201, USA

8 \*Corresponding Author: [mathew.snow@inl.gov](mailto:mathew.snow@inl.gov)

9 Present Phone Number: (208) 526-2966

10 Present Address: PO Box 1625, Idaho Falls, ID 83415-2805, USA

11  
12 For Submission To

13 *Applied Radiation and Isotopes*  
14  
15  
16

# 17 High Purity Sc-47 Production Using High Energy Photons and Natural 18 Vanadium Targets

19 Mathew S. Snow<sup>a\*</sup>, Ari Foley<sup>a</sup>, Jessica L. Ward<sup>a</sup>, Mathew T. Kinlaw, Jon Stoner<sup>b</sup>, Kevin P. Carney<sup>a</sup>

20 a-Idaho National Laboratory, 1765 N. Yellowstone Hwy, Idaho Falls, ID, 83415. United States of  
21 America

22 b-Idaho Accelerator Center, 1500 Alvin Ricken Drive, Pocatello, ID 83201, United States of America

23 Corresponding Author: [mathew.snow@inl.gov](mailto:mathew.snow@inl.gov) (208) 526-2966

24

## 25 Abstract:

26 Scandium-47 (<sup>47</sup>Sc) is of high value for targeted radiotherapy and theranostics; we report a novel, cost-  
27 effective approach to produce high-purity <sup>47</sup>Sc via photonuclear reactions with natural vanadium.  
28 Irradiation at 20 MeV photon end-point energy produces > 99.998% pure <sup>47</sup>Sc, while irradiation at 38  
29 MeV produces 98.8 ± 1.6% pure <sup>47</sup>Sc. Experimental data suggest producing greater than 100 mCi (3700  
30 MBq) of <sup>47</sup>Sc using this approach may be feasible. Future research into refinement and scale-up to  
31 support pre-clinical research is recommended.

32

## 33 Highlights:

- 34 • Photon irradiation of natural vanadium is a novel and inexpensive approach
- 35 • > 99.998% pure <sup>47</sup>Sc is produced at photon energies below 20 MeV
- 36 • Production of > 100 mCi (3700 MBq) of 98.8-99.998% <sup>47</sup>Sc feasible via this approach

37

38 **Keywords:** Sc-47, bremsstrahlung, photonuclear, isotope production, theranostics, cancer therapy

39

## 40 1 Introduction:

41 In recent years, nuclear medicine has sought to combine non-invasive imaging with individual, radiation-  
42 based treatment [Domnanich 2017, Muller 2014, Velikyan 2012, Qaim 2019]. Scandium-47 (<sup>47</sup>Sc) has  
43 been identified as an isotope of considerable value for this application [Qaim 2018, IAEA 2016].  
44 Scandium-47's decay properties, including its short half-life (3.35 d), low-energy β<sup>-</sup> emission (average  
45 energy 162 keV, 100% branching intensity) and low-energy gamma emission (159.4 keV, 68.3%  
46 branching intensity) make it an optimal choice for targeted radiotherapy while simultaneously allowing  
47 for imaging using single-photon emission computed tomography (SPECT) or similar techniques [Pupillo  
48 2019, Jafari 2019, Kolsky 1998, Qaim 2019]. Furthermore, when utilized independently or in conjunction  
49 with other chemically similar, positron emitting isotopes of scandium (e.g., <sup>43</sup>Sc, <sup>44m</sup>Sc, and <sup>44g</sup>Sc), <sup>47</sup>Sc  
50 can be employed as a theranostic (e.g., part of a “matched pair” of diagnostic and therapeutic  
51 radioisotopes that exploit the same molecular targeting vectors) [Domnanich 2017, Baum 2012, Qaim  
52 2018, Qaim 2019]. Additional advantages to radiotherapeutic application of <sup>47</sup>Sc have been suggested,  
53 including a lower dose burden to the patient and potentially greater suitability for small-molecular-weight  
54 and peptide based targeting applications than <sup>177</sup>Lu [Polosak 2013, Muller 2014, Rotsch 2018].

55 Despite its potential value as a radiotherapeutic and radiotheranostic isotope, methods for producing  $^{47}\text{Sc}$   
56 to date have been challenged with achieving the quantities and radio-isotopic purity needed to support  
57 pre-clinical research. The production of  $^{47}\text{Sc}$  in a “carrier-free” form may also be desired in order to  
58 facilitate maximization of the specific activity available for each dose while simultaneously minimizing  
59 potential undesirable physiological side-effects [Kolsky 1998, Yagi 1977]. Numerous groups have  
60 explored irradiations of natural titanium and calcium targets using neutrons [Mausner 1998, Kolsky 1998,  
61 Srivastava 2011, Muller 2014], high-energy photons [Loveless 2019, Rotsch 2018, Starovoitova 2015a,  
62 Starovoitova 2015b, Yagi 1977, Khandaker 2009, Mamtimin 2015], protons [Misiak 2017, Mausner  
63 1998, Kolsky 1998, Srivastava 2011, Pupillo 2019] and other charged particles [Minegishi 2016];  
64 however, each of these routes is limited by the simultaneous production of potentially hazardous, long-  
65 lived  $^{46}\text{Sc}$  ( $t_{1/2} = 83.8$  day, 889.3/1120.5 keV gamma emissions) and/or  $^{48}\text{Sc}$  ( $t_{1/2} = 43.7$  hours, 983.5,  
66 1037.5, 1312 keV gamma emissions). To improve the radiopurity of the final product, many groups have  
67 turned to using enriched Ca and Ti targets [Srivastava 2011, Yagi 1977, Domnanich 2017, Mamtimin  
68 2015]. While successful in achieving higher  $^{47}\text{Sc}$  radio-isotopic purities (when the production techniques  
69 are combined with chemical separations), the enriched target approach suffers from extremely high prices  
70 and limited availability of enriched Ca and Ti isotopes worldwide. Furthermore, even with enriched  
71 targets measurable quantities of  $^{46}\text{Sc}$  and  $^{48}\text{Sc}$  are frequently reported or anticipated [Misiak 2017,  
72 Srivastava 2012, Mamtimin 2015].

73 To address these challenges, we propose a new approach to produce extremely high-purity  $^{47}\text{Sc}$ ; this  
74 approach couples high-energy photons and natural vanadium targets to produce  $^{47}\text{Sc}$  via the  $^{51}\text{V}(\gamma,\alpha)^{47}\text{Sc}$   
75 reaction. Natural vanadium is composed of 99.750%  $^{51}\text{V}$  [Baum 2009] and thus eliminates the need for  
76 enriched targets. Natural vanadium can be easily obtained in large quantities and high chemical purity  
77 from most major chemical suppliers, thereby eliminating supply issues associated with enriched targets.  
78 The cost of natural vanadium is also significantly lower than that of enriched targets, with the cost of  
79 vanadium metal at the time of this writing at ~\$30/g (Aldrich) as compared with \$5,000/g, \$10,000/g and  
80 \$80,000/g for enriched  $^{48}\text{Ti}$  (Isoflex),  $^{50}\text{Ti}$  (Isoflex), and  $^{46}\text{Ca}$  targets (NIDC), respectively. While to our  
81 knowledge this work represents the first rigorous analysis of  $^{47}\text{Sc}$  production via  $^{51}\text{V}(\gamma,\alpha)^{47}\text{Sc}$  reactions  
82 (with a US Patent Application in process) [Snow and Kinlaw 2019], similar efforts utilizing proton  
83 irradiations of natural vanadium are currently being performed in parallel to this work [Pupillo 2019,  
84 Jafari 2019].

85 We report a new method for producing extremely high-purity  $^{47}\text{Sc}$  via photon irradiation of natural  
86 vanadium targets. A series of calculations using published cross-section data and Monte Carlo  
87 simulations utilizing a single accelerator configuration was performed to estimate anticipated trends in the  
88 optimal end-point energy range for maximizing  $^{47}\text{Sc}$  production while simultaneously minimizing  
89 production of other impurities, most notably  $^{46}\text{Sc}$  and  $^{48}\text{Sc}$ . A series of experimental irradiations are also  
90 reported to experimentally evaluate the  $^{47}\text{Sc}$  production quantities and purities that are achievable using  
91 the natural vanadium-photonuclear approach.

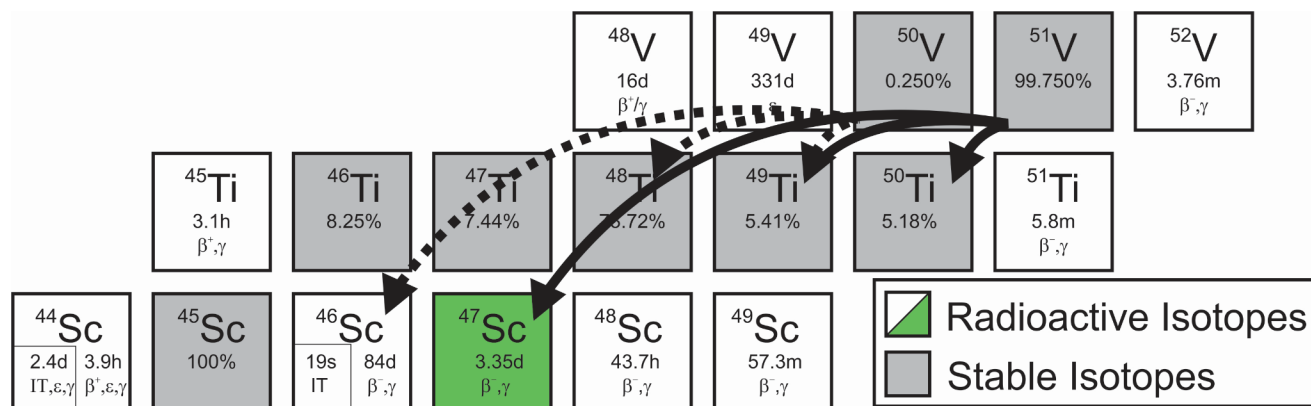
92

93

94

95

96



97

98 **Figure 1.** Chart of the Nuclides plot illustrating the major isotopes that are produced via irradiation of natural  
 99 vanadium targets at photon energies below approximately 20 MeV; gamma-neutron reactions producing vanadium  
 100 isotopes and other isotopes produced at energies above 20 MeV have been omitted for clarity. Solid black lines  
 101 represent the primary isotopes produced from the major isotope  $^{51}\text{V}$  (99.750% abundance); dashed lines represent  
 102 isotopes anticipated to be produced from the minor  $^{50}\text{V}$  isotope (0.250% abundance). Note that, with the exception  
 103 of potential trace  $^{46}\text{Sc}$ , all other titanium and vanadium isotopes produced can be chemically isolated from the  
 104 radioscandium. (see also Figure 2 for a plot of the cross sections for other radioscandium isotope reactions that are  
 105 predicted to occur at end-point energies above 20 MeV).

106

## 107 2 Methods:

108 All chemicals utilized in this work were trace metals grade or better. Natural vanadium metal foils  
 109 (99.99% elemental purity, Goodfellow Corporation) were utilized as accelerator targets.

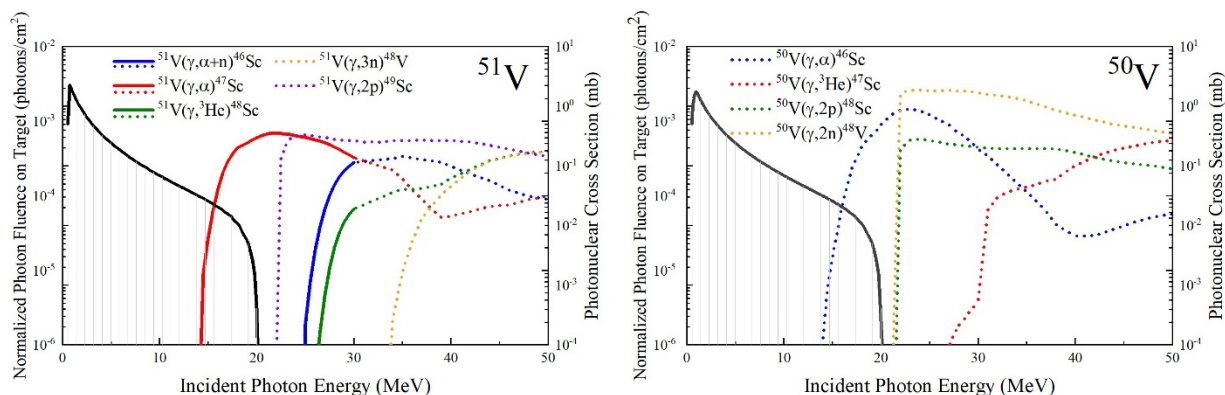
110

### 111 2.1 Calculated Production Based on Published Cross Sections

112 To estimate the relative production rates of  $^{47}\text{Sc}$ ,  $^{46}\text{Sc}$ , and  $^{48}\text{Sc}$  that may be anticipated as a function of  
 113 the bremsstrahlung photon end-point energy, a high-fidelity model of the target, cooling system, and the  
 114 electron-to-photon converter geometry and materials of the Idaho State University's (ISU) Idaho  
 115 Accelerator Center's (IAC) high-power S-band electron linear accelerator (LINAC) was developed using  
 116 the Monte Carlo N-Particle (MCNP6) Code. The electron beam was modeled as a forward-projecting  
 117 source with a radius of 0.15 cm that impinged on a series of water-cooled tungsten converter foils. A  
 118 natural vanadium foil was modeled as a 0.125 mm thick, 1.99 cm<sup>2</sup> foil (mass 0.152 g) placed inside a  
 119 water-cooled irradiation capsule representative of the design utilized during the 38 MeV irradiation  
 120 experiment. Photonuclear cross section data for photon energies from 0 to 30 MeV were obtained from  
 121 the Evaluated Nuclear Data File database (ENDF/B-VIII.0) [Brown 2018]; for energies above 30 MeV  
 122 where no ENDF/B-VIII.0 cross sections were available, data were supplemented using the Japanese  
 123 Evaluated Nuclear Data Library (JENDL) photonuclear data file (JENDL/PD-2016) [Iwamoto 2016]. A  
 124 linear interpolation was utilized to combine data between the ENDF/B-VIII.0 cross section that ends at 30  
 125 MeV and the JENDL/PD-2016 cross section beginning at 32 MeV. The combination of ENDF/B-VIII.0  
 126 and JENDL/PD-2016 photonuclear cross section data utilized in the production estimates is shown in  
 127 Figure 2.

128 The photonuclear reactions considered in the calculations represent the primary hypothesized production  
 129 pathways for producing  $^{46}\text{Sc}$ ,  $^{47}\text{Sc}$ ,  $^{48}\text{Sc}$ , and  $^{49}\text{Sc}$  from  $^{51}\text{V}$  and  $^{50}\text{V}$ ; the specific reactions considered in

130 this work include  $^{51}\text{V}(\gamma,\alpha)^{47}\text{Sc}$ ,  $^{51}\text{V}(\gamma,\alpha+n)^{46}\text{Sc}$ ,  $^{51}\text{V}(\gamma,^3\text{He})^{48}\text{Sc}$ ,  $^{51}\text{V}(\gamma,2p)^{49}\text{Sc}$ ,  $^{51}\text{V}(\gamma,3n)^{48}\text{V}$ ,  $^{50}\text{V}(\gamma,\alpha)^{46}\text{Sc}$ ,  
 131  $^{50}\text{V}(\gamma,^3\text{He})^{47}\text{Sc}$ , and  $^{50}\text{V}(\gamma,2p)^{48}\text{Sc}$ . Potential  $^{46}\text{Sc}$ ,  $^{47}\text{Sc}$ ,  $^{48}\text{Sc}$ ,  $^{49}\text{Sc}$ , or  $^{48}\text{V}$  production pathways that require  
 132 multiple reactions (e.g., two sequential  $(\gamma,np)$  or similar reactions with titanium isotope intermediates,  
 133 etc.) were not included in the calculations as these reactions are anticipated to produce insignificant  
 134 quantities of radioactive scandium and vanadium isotopes relative to the other production pathways.



135  
 136 **Figure 2.** Comparison of published photonuclear cross sections as a function of the incident photon energy for (left)  
 137  $^{51}\text{V}$  (99.750% abundance in natural vanadium) and (right)  $^{50}\text{V}$  (0.250% abundance). Colored lines represent cross  
 138 section data for  $^{47}\text{Sc}$  production (red),  $^{46}\text{Sc}$  production (blue),  $^{48}\text{Sc}$  production (green),  $^{49}\text{Sc}$  (violet), and  $^{48}\text{V}$   
 139 production (yellow) accessed from ENDFB/VIII.0 (bold lines) and JENDL/PD-2016 (dotted lines). Black lines  
 140 represent the energy distribution of the photon fluence on the natural vanadium targets for a typical 20 MeV end-  
 141 point bremsstrahlung photon beam (see Figure SI-1, Supplementary Information, for the predicted bremsstrahlung  
 142 photon fluence at higher the electron end-point energy).

143  
 144 **2.2 Irradiation Experiments**

145 A series of irradiation experiments were performed to experimentally evaluate the relative production of  
 146  $^{46}\text{Sc}$ ,  $^{47}\text{Sc}$  and  $^{48}\text{Sc}$  as a function of the bremsstrahlung photon end-point energy. For these experiments,  
 147 natural vanadium targets (0.125 mm thickness) with masses ranging from 0.1520 to 0.4630 g were  
 148 utilized as the target materials. Irradiations were performed using three different electron LINACs at the  
 149 IAC. Irradiations at 20 MeV bremsstrahlung photon end-point energies were performed using the IAC 25  
 150 MeV S-band electron linear accelerator, while those at 22 and 26 MeV utilized the 44 MeV L-band  
 151 electron linear accelerator. An additional irradiation at 38 MeV was performed using the high-power S-  
 152 band LINAC.

153 For irradiations using the 25 MeV S-band LINAC, high-energy electrons from the LINAC were impinged  
 154 on a 4.9 g/cm<sup>2</sup> tungsten converter positioned 2.1 cm from the end of the accelerator beam pipe. To  
 155 maximize the photon flux on target, samples were positioned directly at the face of the tungsten converter.  
 156 Targets were irradiated for 1 hour at an end-point energy of 20 MeV with an average current of  
 157 approximately 33 microamps. Within 30 minutes of the end of the irradiation the foil was analyzed via  
 158 gamma spectrometry.

159 For the irradiation experiments utilizing the 44 MeV L-band LINAC, two separate 0.44 to 0.46 g natural  
 160 vanadium targets were placed on the face of the tungsten converter at the end of the accelerator beam  
 161 pipe. Each target was irradiated at either a 22 MeV or 26 MeV end-point energy for 10 minutes at an  
 162 average current of approximately 49.5 and 75 microamps (respectively). After the irradiation each

163 vanadium foil was allowed to cool for several minutes prior to analysis via gamma spectrometry.

164 For the irradiation experiment utilizing the 38 MeV high-power S-band accelerator, a 0.1520 g vanadium  
165 foil was placed inside a water-cooled sample holder and irradiated for 1 hour at an electron energy of 38  
166 MeV and an average current of approximately 198 microamps. Due to the high radiation dose in the  
167 irradiation hall following the 1 hour irradiation the vanadium foil was allowed to decay overnight prior to  
168 gamma spectrometry analysis.

169

## 170 2.5 Gamma Spectrometry Analysis

171 Gamma spectrometry analyses were performed using either a Canberra model GC3318 n-type high-purity  
172 germanium (HPGe) detector or a mechanically-cooled Ortec GMX n-type HPGe detector. Detector  
173 calibrations on both systems were performed using a series of National Institutes of Standards and  
174 Technology (NIST) traceable gamma-ray spectrometry calibration sources (CAL2600, North American  
175 Scientific; GF-057-M, Eckert and Ziegler; 2600, Eckert and Ziegler). Immediately prior to the  
176 irradiations, energy and efficiency calibrations were performed on the HPGe detectors, and energy  
177 calibrations were further verified during the experiments for any calibration shifts. Samples were placed  
178 at either 6 cm or 15 cm from the face of the detector to ensure detector dead times remained less than 5%.  
179 Measurements for quantitative  $^{47}\text{Sc}$  determination were performed at 15 cm from the detector face to  
180 minimize systematic bias to the data between the different geometries of the gamma calibration sources  
181 and samples. Sample activities were corrected to the end-of-bombardment (EOB). Detection limits for  
182 non-detected radionuclides were calculated using the method of Gilmore and are reported at the 95%  
183 confidence level [Gilmore 2008].

184

185

186

187

188

189

190

191

192

193

194

195

196

197

198

199

200

## 201 3 Results:

### 202 3.1 Calculated Production Based on Published Cross Sections

203 A visual comparison of the bremsstrahlung photon fluence and empirical cross section data, obtained  
204 from ENDF/B-VIII.0 and JENDL/PD-2016, as a function of the photon energy is shown in Figure 2. A  
205 negative Q-value, calculated by the difference in the rest masses of the reaction constituents, reflects the  
206 minimum required kinetic energy for the reaction to occur. The Q-value of the  $^{51}\text{V}(\gamma,\alpha)^{47}\text{Sc}$  reaction is  
207 reported by the National Nuclear Data Center to be -10.292 MeV [QCALC]; the ENDF/B-VIII.0 cross  
208 section has the first non-zero value at 14 MeV (0.289  $\mu\text{barns}$ ) and reaches a maximum of approximately  
209 0.35 mbarns at 22 MeV as illustrated in Figure 2 [ENDF/B-VIII.0]. The production of  $^{46}\text{Sc}$  via  
210  $^{50}\text{V}(\gamma,\alpha)^{46}\text{Sc}$  is reported to follow a qualitatively similar trend, with a Q-value of -9.887 MeV [QCALC], a  
211 sharp increase in the reported cross section data beginning at approximately 13.5 MeV and a maximum  
212 average cross section of approximately 0.8 mbarn at 22.5 MeV [JENDL/PD-2016]. The Q-value for the  
213  $^{51}\text{V}(\gamma,\alpha+n)^{46}\text{Sc}$  reaction is -21.674 MeV [QCALC]; the reaction cross section is reported to exhibit a sharp  
214 increase at approximately 26.5 MeV and reach a maximum of approximately 0.1 mbarn at 36 MeV  
215 [JENDL/PD-2016]. The Q-value of the  $^{51}\text{V}(\gamma,2p)^{49}\text{Sc}$  reaction is -20.221 MeV [QCALC], with the  
216 JENDL/PD-2016 cross section reporting the first non-zero value at 22.57 MeV (0.1288 mbarns)  
217 [JENDL/PD-2016]. As illustrated in Figure 2, other reactions including  $^{51}\text{V}(\gamma,^3\text{He})^{48}\text{Sc}$ ,  $^{50}\text{V}(\gamma,^3\text{He})^{47}\text{Sc}$   
218 and  $^{50}\text{V}(\gamma,2p)^{48}\text{Sc}$ , are predicted to become more prevalent as the photon energy increases above  
219 approximately 26 MeV.

220 Several qualitative observations can be made by evaluating the bremsstrahlung photon fluence profile and  
221 by comparing trends in empirical cross section data (with an understanding that the photonuclear cross  
222 section data for ENDF/B-VIII.0 is incomplete and not always in quantitative agreement with  
223 JENDL/PD-2016 values; experimental validation is thus required for quantitative evaluation). First, a  
224 comparison of the thresholds and general profiles of the  $^{51}\text{V}(\gamma,\alpha)^{47}\text{Sc}$  and  $^{50}\text{V}(\gamma,\alpha)^{46}\text{Sc}$  reaction cross  
225 sections suggests that in the absence of an isotopically pure  $^{51}\text{V}$  target some  $^{46}\text{Sc}$  production is predicted  
226 to be inevitable regardless of the bremsstrahlung photon end-point energy. Fortunately, natural vanadium  
227 is 99.750%  $^{51}\text{V}$  and thus the  $^{50}\text{V}(\gamma,\alpha)^{46}\text{Sc}$  reaction is minimized substantially by simply using natural  
228 vanadium targets. This is illustrated by the MCNP6 model and subsequent calculations, the results of  
229 which are shown in Table 1.  $^{46}\text{Sc}$  and  $^{48}\text{Sc}$  production from natural vanadium targets irradiated at  
230 bremsstrahlung photon end-point energies less than 20 MeV are predicted to represent < 0.01% of the  
231 total radioactive scandium activity at the EOB. As the end-point energy increases beyond 20 MeV the  
232 quantity of  $^{46}\text{Sc}$  and  $^{48}\text{Sc}$  is predicted to increase relative to  $^{47}\text{Sc}$ .  $^{49}\text{Sc}$  production is also predicted to  
233 increase substantially at end-point energies above 20 MeV and is predicted to potentially dominate the  
234 overall radioscandium activity at EOB when irradiated at energies above 20 MeV.  $^{49}\text{Sc}$  is a high energy  $\beta^-$   
235 emitting isotope and thus could be significantly detrimental to therapeutic applications if present in the  
236 final purified samples; fortunately,  $^{49}\text{Sc}$  exhibits a 57.3 minute half life and thus decays rapidly. For  
237 irradiations above 20 MeV photon energies, allowing the sample to decay for roughly 20 or so hours prior  
238 to application results in a decrease in  $^{49}\text{Sc}$  content to sub 0.02% levels of the total radioscandium activity  
239 (see Figure SI-2, Supplementary Information Section). Finally, it is worth noting that production of  $^{48}\text{V}$   
240 and  $^{49}\text{V}$  through the  $^{50}\text{V}(\gamma,2n)$ ,  $^{51}\text{V}(\gamma,3n)$ ,  $^{50}\text{V}(\gamma,n)$ , and  $^{51}\text{V}(\gamma,2n)$  reaction pathways is predicted to occur at  
241 energies greater than approximately 21 MeV and 32 MeV, respectively, though as with the various  
242 titanium isotopes that are produced through  $(\gamma,p)$  and  $(\gamma,np)$  reactions,  $^{48,49}\text{V}$  can be chemically separated  
243 from the radioactive scandium product.

244 A final, important aspect when considering the modeling data in Table 1 is that these calculations used  
245 published cross section data combined with the measured irradiation parameters (e.g., repetition rate,

246 average electron beam charge, geometry, target mass) utilized in the 38 MeV S-band high-power  
 247 accelerator, whereas the experimental data provided hereafter in section 3.2 was produced using 3  
 248 different accelerator systems. The use of 3 different accelerator systems for the experimental irradiations  
 249 was necessary due to practical limitations in the end-point energy ranges available for different  
 250 accelerators at IAC at the time of this work. Rather than report model predictions for each accelerator, a  
 251 single accelerator/experiment configuration is intentionally reported in this section in order to provide a  
 252 single, self-consistent dataset that enables a qualitative comparison of the relative activity distributions of  
 253 different scandium isotopes that are predicted (based upon available cross section data) as a function of  
 254 the bremsstrahlung end-point energy. The data provided in Table 1 is thus intended to show the general  
 255 trends anticipated at different end-point energies; for quantitative prediction of scandium isotope  
 256 production for the 20, 22, and 26 MeV irradiations performed in this work, or for future irradiations on  
 257 different electron linear accelerators, a rigorous model of each of these systems and target configurations  
 258 is necessary.

259

260 **Table 1:** MCNP6-based radioactive scandium production estimates for a 0.152 g natural vanadium target irradiated  
 261 for 1 hour at an average current of approximately 198 microamps.

Bremsstrahlung End-point Energy (MeV)	% Radioscandium Activity at End-of-Bombardment				% Radioscandium Activity at 20 Hours Post-irradiation			
	% <sup>47</sup> Sc	% <sup>46</sup> Sc	% <sup>48</sup> Sc	% <sup>49</sup> Sc	% <sup>47</sup> Sc	% <sup>46</sup> Sc	% <sup>48</sup> Sc	% <sup>49</sup> Sc
14	99.9945%	0.0055%	0.000%	0.000%	99.994%	0.006%	0.000%	0.000%
20	99.9909%	0.0090%	0.000%	0.0002%	99.989%	0.011%	0.000%	0.0003%
26	15.9168%	0.0027%	0.0112%	84.0693%	99.919%	0.020%	0.061%	0.020%
30	5.5914%	0.0023%	0.0125%	94.3937%	99.756%	0.048%	0.194%	0.001%
38	3.2504%	0.0117%	0.088%	96.6499%	97.307%	0.412%	2.288%	0.002%

262

263

264

265

266

267

268

269

270

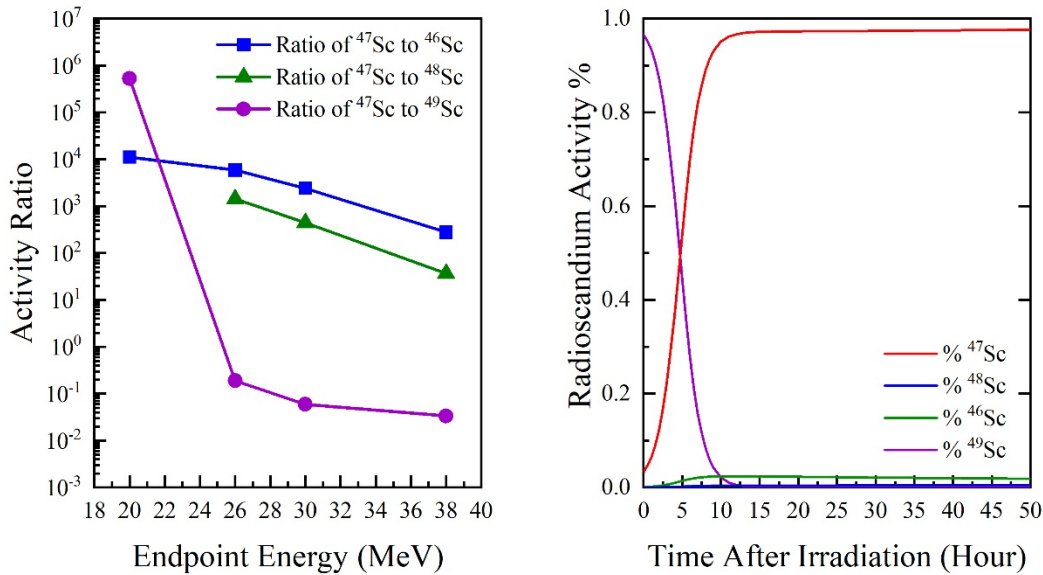
271

272

273

274

275 **Figure 3.** (left) MCNP6-based prediction of the  $^{47}\text{Sc}/^{46}\text{Sc}$ ,  $^{47}\text{Sc}/^{48}\text{Sc}$ , and  $^{47}\text{Sc}/^{49}\text{Sc}$  activity ratios at EOB as a  
 276 function of the bremsstrahlung photon end-point energy. (right) Visualization of calculated  $^{47}\text{Sc}$ ,  $^{46}\text{Sc}$ ,  $^{48}\text{Sc}$ , and  $^{49}\text{Sc}$   
 277 activity % (by % of total radioscandium) with respect to time following irradiation at 38 MeV bremsstrahlung  
 278 photon endpoint energy. For irradiations above 20 MeV where  $^{49}\text{Sc}$  production is predicted to become significant,  
 279 waiting ~20 hours to allow the  $^{49}\text{Sc}$  to decay is predicted to enable minimization of this isotope, thereby producing a  
 280 residual high purity  $^{47}\text{Sc}$  solution.



281

282

283

284

### 285 3.2 Bremsstrahlung Irradiation Experiments at 20, 22, 26 and 38 MeV Bremsstrahlung Photon End-point 286 Energies

287 Gamma spectrometry data from the various irradiation experiments are shown in Table 2, with plots of  
 288 the gamma spectra given in Figure 4. Irradiation at 20 MeV produced no measurable quantity of  $^{46}\text{Sc}$  or  
 289  $^{48}\text{Sc}$ ; based on the gamma spectrometry detection limits for these experiments the maximum  $^{46}\text{Sc}$  content  
 290 in this samples represents <0.002% of the total radioscandium at EOB at this end-point energy. The  
 291 irradiations at 22 and 26 likewise produced no detectable  $^{46}\text{Sc}$  or  $^{48}\text{Sc}$ .  $^{49}\text{Sc}$  was also not detected by  
 292 gamma spectrometry during any irradiations, though this result is not surprising as  $^{49}\text{Sc}$  has a very low  
 293 gamma emission rate (0.05% branching intensity at 1761.971 keV). At the 38 MeV bremsstrahlung  
 294 photon end-point energy measurable quantities of  $^{46}\text{Sc}$  and  $^{48}\text{Sc}$  are observed as predicted; however, even  
 295 at this energy these isotopes represent a minor component to the overall measured radioactive scandium  
 296 activity (only  $0.60 \pm 0.02\%$  and  $0.55 \pm 0.02\%$  of the total radioscandium activity at EOB, respectively). It  
 297 should be noted that in the 38 MeV irradiation,  $^{48}\text{V}$  was produced at a rate of  $1.372 \pm 0.026 \mu\text{Ci/g V/hr}$ .  
 298 Although predicted to be produced at bremsstrahlung X-ray energies greater than 20 MeV,  $^{49}\text{V}$  ( $T_{1/2}=330$   
 299 days) was not detected as it decays by electron capture with no emitted  $\gamma$ -rays. However, by coupling  
 300 photonuclear production to chemical separations  $^{48}\text{V}$  and  $^{49}\text{V}$  can be isolated along with the bulk V target  
 301 material and thus  $^{48,49}\text{V}$  production should have minimal impact on the final  $^{47}\text{Sc}$  purity.

302

303

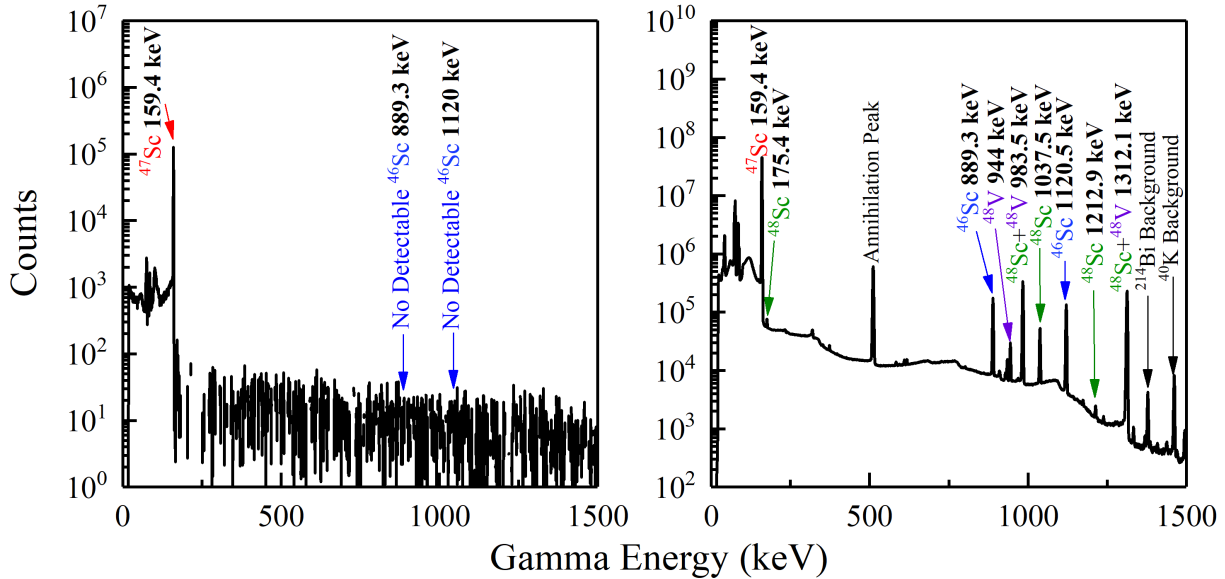
305 Table 2. Experimentally observed <sup>47</sup>Sc, <sup>46</sup>Sc and <sup>48</sup>Sc production rates as a function of different bremsstrahlung  
 306 photon end-point energies on different accelerator systems at IAC. Activities are reported at EOB. Uncertainties  
 307 represent the 95% confidence level.

End-point Energy (MeV) and Accelerator	Target Mass (g)	Rep Rate (Hz)	Average Charge Per Pulse (nC)	Average Current (μA)	<sup>47</sup> Sc (nCi/μA/hr)	<sup>46</sup> Sc (nCi/μA/hr)	<sup>48</sup> Sc (nCi/μA/hr)	% Activity <sup>47</sup> Sc	% Activity <sup>46</sup> Sc	% Activity <sup>48</sup> Sc
20 MeV on S-Band	0.2381	150	220	33	5.09 ± 0.182	< 4.545E-4	< 4.45E-5	> 99.998%	< 0.001%	< 0.001%
22 MeV on L-Band	0.4460	150	330	49.5	3.27 ± 0.273	< 0.024	< 0.034	> 98.2%	< 0.7%	< 1.1%
26 MeV on L-Band	0.4630	150	500	75	15.2 ± 0.06	< 0.017	< 0.031	> 99.7%	< 0.1%	< 0.2%
38 MeV on High-Power S-band	0.1520	300	660	198	545.5 ± 15.2	3.33 ± 0.10	3.03 ± 0.10	98.8 ± 1.6%	0.60 ± 0.02%	0.55 ± 0.02%

308

309

310



311

312 **Figure 4.** Gamma-ray spectra of natural vanadium targets irradiated at (left) 20 MeV (background-subtracted) and  
 313 (right) 38 MeV bremsstrahlung end-point energies with live-times of these measurements of 17.6 hours and 63.4  
 314 hours, respectively. <sup>47</sup>Sc is the only radioscandium isotope observed above background at 20 MeV, while trace <sup>46</sup>Sc,  
 315 <sup>48</sup>Sc, and <sup>48</sup>V are observed in the 38 MeV irradiation sample.

316

317 **3.3 Potential Options for Future <sup>47</sup>Sc Production Scale-Up**

318

319 Several options are available for increasing <sup>47</sup>Sc production to the 100+ mCi levels (3700+ MBq) needed  
 320 to support pre-clinical trials. The first and simplest option is to increase the mass of the vanadium target  
 321 material that is present within the photon beam. While production is anticipated to scale roughly linearly  
 322 with mass initially, as the mass increases attenuation of the photon beam can result in departure from  
 323 linearity. Experience with isotope production using electron linear accelerators reported in the literature  
 324 suggests that targets as large as 100-200 grams should be feasible for use via the electron linear  
 325 accelerator approach (though logistical constraints such as the size of the target assembly, target cooling,

326 and challenges with subsequent chemical handling represent practical considerations that must be  
327 overcome for large target masses). Methods for dissolving and chemically isolating  $^{47}\text{Sc}$  from targets in  
328 this range presently represents an active area of research. Preliminary model calculations from our team  
329 suggests that scale-up production is feasible for producing mCi quantities of  $^{47}\text{Sc}$  via this approach; a  
330 rigorous analysis of potential scale-up options represents a current research focus. A second option for  
331 accelerator systems with fixed maximum electron current capabilities (such as those employed in this  
332 work) is to utilize higher end-point energies. As illustrated in Figure SI-1, Supplementary Information,  
333 the electron-to-photon conversion ratio increases with increasing electron end-point energy; this in turn  
334 results in a higher photon flux available at all energies below the end-point energy and thus can produce a  
335 higher number of photons within the  $^{51}\text{V}(\gamma,\alpha)^{47}\text{Sc}$  cross section range than an irradiation under similar  
336 conditions but at a lower electron end-point energy. The limitation with this approach, however, is that  
337 the higher energy photons access additional reaction pathways that produce other, undesired scandium  
338 isotopes (e.g.,  $^{46}\text{Sc}$ ,  $^{48}\text{Sc}$ ,  $^{49}\text{Sc}$ ), thereby decreasing the overall  $^{47}\text{Sc}$  product purity. A third (and potentially  
339 optimal) option would be to utilize a purpose built electron linear accelerator that is optimized for high  
340 electron current at lower end-point energies (possibly in the 20-30 MeV range). Such a system would  
341 enable maximization of the photon flux within the  $^{51}\text{V}(\gamma,\alpha)^{47}\text{Sc}$  cross section range without producing  
342 other side product isotopes.  
343

344 While this study was constrained in the total current able to be achieved in the 20-30 MeV end-point  
345 energy range (due to limitations in the maximum current achievable by the systems available for research  
346 at the time), the data from the irradiation at 38 MeV appears particularly promising for the potential  
347 applicability of the electron linear accelerator-natural vanadium target approach for producing therapeutic  
348 levels of  $^{47}\text{Sc}$ . The measured  $^{47}\text{Sc}$  production rate at the 38 MeV end-point energy was  $108 \pm 3 \mu\text{Ci/g/hr}$ ;  
349 given linear scaling with increasing mass (first approximation), then increasing the target mass to 100 g  
350 and irradiation time to 10 hours would result in the production of  $\sim 100 \text{ mCi}$  ( $\sim 3700 \text{ MBq}$ ) of 98.8% pure  
351  $^{47}\text{Sc}$ . This is within the range for a standard therapeutic dose for  $^{177}\text{Lu}$  (a potential analog for  $^{47}\text{Sc}$ ). While  
352 additional research is needed to demonstrate these production levels, these results strongly indicate the  
353 potential viability for the natural vanadium pathway to produce the large quantities and purity of  $^{47}\text{Sc}$   
354 needed to support future pre-clinical research efforts.

355

#### 356 **4 Conclusions:**

357 Irradiation of natural vanadium targets using electron linear accelerators offers an attractive option for  
358 producing extremely high-purity, carrier-free  $^{47}\text{Sc}$ . The low cost and wide availability of natural  
359 vanadium presents significant advantages over the enriched Ti and Ca approaches. Irradiation at 20 MeV  
360 bremsstrahlung end-point energies produces extremely high-purity  $^{47}\text{Sc}$  ( $> 99.998\%$  pure) at EOB. At  
361 photon energies above 20 MeV the  $^{51}\text{V}(\gamma,2p)^{49}\text{Sc}$  reaction is predicted to dominate the overall  
362 radioscandium activity, however as  $^{49}\text{Sc}$  has a 57.3 minute half life  $^{49}\text{Sc}$  can be eliminated from samples  
363 irradiated above 20 MeV by simply allowing the sample to cool for several hours prior to use. The  
364 experimental irradiation at 38 MeV results in significantly higher production of  $^{47}\text{Sc}$  ( $108 \pm 3 \mu\text{Ci/g/hr}$ ),  
365 primarily due to the production cross section and current available in the experimental systems utilized,  
366 albeit at slightly lower overall total radioscandium purity ( $98.8 \pm 1.6\%$   $^{47}\text{Sc}$ ). These data indicate that,  
367 given continued research and method development focused on scaling-up, the production of 100 mCi  
368 ( $3700 \text{ MBq}$ ) quantities needed to provide a therapeutic dose of  $^{47}\text{Sc}$  may be possible using this approach.  
369 For irradiations at 20 MeV in particular, the potential for  $^{47}\text{Sc}$  production using high current accelerators  
370 located on-site at nuclear medicine facilities may enable the use of this reaction for providing local “dose-  
371 on-demand.” Future research into methods to further optimize the production quantities,  $^{47}\text{Sc}$  purity, and  
372 chemical approaches to refine separations, is recommended.

373

374

375 **Acknowledgements**

376 The authors would like to thank Dr. Steven Hartenstein for his advice and guidance with this work, Dr.  
377 Erin Searcy and Dr. Marianne Walck for their technical comments and direction with regards to funding  
378 support, Dr. Edna Cardenas and Dr. Brian Bucher for their technical advice and reviews of the data and  
379 Mr. Hayden Town for assistance with technical editing. The authors also want to thank the Idaho  
380 Accelerator Center staff, Kevin Folkman, Chad O’Neil, Brian Berls, and John Longley for their help in  
381 performing the experiments. This work was supported through the Idaho National Laboratory Directed  
382 Research & Development (LDRD) Program under DOE Idaho Operations Office Contract DE-  
383 AC07-05ID14517. Neither the U.S. Government nor any agency thereof, nor any of their employees,  
384 makes any warranty, express or implied, or assumes any legal liability or responsibility for the accuracy,  
385 completeness, or usefulness of any information, apparatus, product, or process disclosed, or represents  
386 that its use would not infringe on privately owned rights. References herein to any specific commercial  
387 product, process, or service by trade name, trademark, manufacturer, or otherwise, does not necessarily  
388 constitute or imply its endorsement, recommendation, or favoring by the U.S. Government or any agency  
389 thereof. Views and opinions of the authors expressed herein do not necessarily reflect those of the U.S.  
390 Government or any agency thereof. This research also made use of the resources at the High Performance  
391 Computing Center at Idaho National Laboratory, which is supported by the Office of Nuclear Energy of  
392 the U.S. Department of Energy and the Nuclear Science User Facilities under Contract No. DE-  
393 AC07-05ID14517.

394

395

396

397

398

399

400

401

402

403

404

405

406

407

408

409

410

411

412 **References:**

413 Baum, E.M.; Ernesti, M.C.; Knox, H.D.; Miller, T.R.; Watson, A.M. 2009. Nuclides and Isotopes Chart  
414 of the Nuclides, Seventeenth Edition. Bechtel Marine Propulsion Corporation, ISBN  
415 978-0-9843653-0-2.

416 Baum, R.P., Kulkarni, H.R., 2012. Theranostics: From Molecular Imaging Using Ga-68 Labeled Tracers  
417 and PET/CT to Personalized Radionuclide Therapy – The Bad Berka Experience. *Theranostics*, 2(5):437.

418 Brown, D.A.; Chadwick, M.B.; Capote, R.; Kahler, A.C.; Trkov, A.; Herman, M.W.; Sonzogni, A.A.;  
419 Danon, Y.; Carlson, A.D.; Dunn, M.; Smith, D.L.; Hale, G.M.; Arbanas, G.; Arcilla, R.; Bates, C.R.;  
420 Beck, B.; Becker, B.; Brown, F.; Casperson, R.J.; Conlin, J.; Cullen, D.E.; Descalle, M.-A.; Firestone, R.;  
421 Gaines, T.; Guber, K.H.; Hawari, A.I.; Holmes, J.; Johnson, T.D.; Kawano, T.; Kiedrowski, B.C.;  
422 Koning, A.J.; Kopecky, S.; Leal, L.; Lestone, J.P.; Lubitz, C.; Marquez Damian, J.I.; Mattoon, C.M.;  
423 McCutchan, E.A.; Mughabghab, S.; Navratil, P.; Neudecker, D.; Nobre, G.P.A.; Noguere, G.; Paris, M.;  
424 Pigni, M.T.; Plompen, A.J.; Pritychenko, B.; Pronyaev, V.G.; Roubtsov, D.; Rochman, D.; Romano, P.;  
425 Schillebeeckx, P.; Simakov, S.; Sin, M.; Sirakov, I.; Sleaford, B.; Sobes, V.; Soukhovitski, E.S.; Stetcu,  
426 I.; Talou, P.; Thompson, I.; van der Marck, S.; Welser-Sherrill, L.; Wiarda, D.; White, M.; Wormald, J.L.;  
427 Wright, R.Q.; Zerkle, M.; Zerovnik, G.; Zhu, Y., 2018. ENDF/B-VIII.0: The 8<sup>th</sup> major release of the  
428 nuclear reaction data library with CIELO-project cross sections, new standards and thermal scattering  
429 data. *Nucl. Data Sheets*, 148, 1.

430 Data produced by the code QCALC, written by T.W. Burrows, National Nuclear Data Center,  
431 Brookhaven National Laboratory, and based on the AME2016 atomic mass evaluation (II), Meng  
432 et al, *Chinese Physics C* Vol. 41, No 3 (2017).

433 Domnanich, K. A.; Muller, C.; Benesova, M.; Dressler, R.; Haller, S.; Koster, U.; Ponsard, B.; Schibli,  
434 R.; Turler, A.; van der Meulen, N.P., 2017. <sup>47</sup>Sc as useful β<sup>-</sup> emitter for the radiotheragnostic paradigm: a  
435 comparative study of feasible production routes. *EJNMMI Radiopharmacy and Chemistry* 2:5.

436 Gilmore, G. 2008. *Practical Gamma-ray Spectrometry*, 2nd Edition. John Wiley & Sons, Ltd. ISBN:  
437 978-0-470-86196-7

438 IAEA 2016. CRP on therapeutic radiopharmaceuticals labelled with new emerging radionuclides (<sup>67</sup>Cu,  
439 <sup>186</sup>Re, <sup>47</sup>Sc), No. F22053, 2016-2020. <http://cra.iaea.org/cra/explore-crps/all-active-by-programme.html>

440 Iwamoto, O.; Sanami, T.; Kunieda, S.; Koura, H.; Nakamura, S., 2016. Photonuclear Data File, JAEA-  
441 Conf 2016-004, 53-58.

442 Jafari, A.; Aboudzadeh, M.R.; Azizakram, H.; Sadeghi, M.; Alirezapour, B.; Rajabifar, S.; Yousefi, K.,  
443 2019. Investigations of proton and deuteron induced nuclear reactions on natural and enriched Titanium,  
444 Calcium and Vanadium targets, with special reference to the production of <sup>47</sup>Sc. *Applied Radiation and*  
445 *Isotopes*, 152, 145-155.

446 Khandaker, M.; Kim, K.; Lee, M.W.; Kim, K.S.; Kim, G.N.; Cho, Y.S.; Lee, Y.O., 2009. Investigations  
447 of the nat Ti(p,x) (43,44m,44g,46,47,48)Sc, 48V nuclear processes up to 40 MeV. *Appl. Radiat. Isot.* 67,  
448 1348-1354.

449 Kolsky, K.L.; Joshi, V.; Mausner, L.F.; Srivastava, S.C., 1998. Radiochemical purification of no-carrier-  
450 added scandium-47 for radioimmunotherapy. *Appl. Radiat. Isot.* 49, 1541-1549.

451 Loveless, C.S.; Radford, L.L.; Ferran, S.J.; Queern, S.L.; Shepherd, M.R.; Lapi, S.E., 2019. Photonuclear  
452 production, chemistry, and in vitro evaluation of the theranostic radionuclide <sup>47</sup>Sc. *EJNMMI Research*,

453 9:42.

454 Mamtimin, M., Harmon, F., Starovoitova, V.N., 2015. Sc-47 production from titanium targets using  
455 electron linacs. *Appl. Radiat. Isot.* 102, 1-4.

456 Mausner, L.F.; Kolsky, K.L.; Joshi, V.; Srivastava, S.C., 1998. Radionuclide development at BNL for  
457 nuclear medicine therapy. *Appl. Radiat. Isot.*, 49, 285-294.

458 Minegishi, K.; Nagatsu, K.; Fukada, M.; Suzuki, H.; Ohya, T.; Zhang, M.R., 2016. Production of  
459 scandium-43 and -47 from a powdery calcium oxide target via the nat/44Ca(a,x)-channel. *Appl Radiat*  
460 *Isotop* 116, 8-12.

461 Misiak, R.; Walczak, R.; Was, B.; Bartyzel, M.; Mietelski, J.W.; Bilewicz, A., 2017. <sup>47</sup>Sc production  
462 development by cyclotron irradiation of <sup>48</sup>Ca, *J. Radioanal Nucl Chem*, 313, 429-434.

463 Muller, C.; Bunka, M.; Haller, S.; Koster, U.; Groehn, V.; Bernhardt, P.; van er Meulen, N.; Turler, A.;  
464 Schibli, R., 2014. Promising Prospects for 44Sc-47Sc-Based Theragnostics: Application of 47Sc for  
465 Radionuclide Tumor Therapy in Mice. *J. Nucl. Med.*, 55(10), 1568-1664.

466 Polosak, M.; Piotrowska, A.; Krajewski, S.; Bilewicz, A., 2013. Stability of 47Sc-complexes with acyclic  
467 polyamino-polycarboxylate ligands. *J. Radioanal. Nucl. Chem.*, 295, 1867-1872.

468 Pupillo, G.; Mou, L.; Boschi, A.; Calzaferri, S.; Canton, L.; Cisternino, S.; De Dominicis, L.; Duatti, A.;  
469 Fontana, A.; Haddad, F.; Martini, P.; Pasquali, M.; Skliarova, H.; Esposito, J., 2019. Production of 47Sc  
470 with natural vanadium targets: results of the PASTA project. *J. Radioanal. Nucl. Chem.* 322, 1711-1718.

471 Qaim, S.M., Scholten, B., Neumaier, B., 2018. New developments in the production of theranostic pairs  
472 of radionuclides. *J. Radioanal Nucl Chem* 318:1493-1509.

473 Qaim, S.M. 2019. Theranostic radionuclides: recent advances in production methodologies. *J. Radioanal.*  
474 *Nucl. Chem.* 322, 1257-1266.

475 Rotsch D.A.; Brown, M.A.; Nolen, J.A.; Brossard, T.; Henning, W.F.; Chemerisov, S.D.; Gromov, R.G.;  
476 Greene, J., 2018. Electron linear accelerator production and purification of 47Sc from titanium dioxide  
477 targets. *Appl Radiat Isot* 131:77–82.

478 Snow, M.S. and Kinlaw, M.T., 2019. Production of High Purity Scandium-47. Patent Cooperation Treaty  
479 Application PCT/US20/31422, Docket #BA-1094.

480 Srivastava, S.C. 2011. Paving the way to personalized medicine: production of some theragnostic  
481 radionuclides at Brookhaven National Laboratory. *Radiochim. Acta*, 99, 635-640.

482 Srivastava SC. 2012. Paving the way to personalized medicine: production of some promising  
483 theragnostic radionuclides at Brookhaven National Laboratory. *Semin Nucl Med.*, 42(3):151–63.

484 Starovoitova VN, Cole PL, Grimm TL, 2015a. Accelerator-based photoproduction of promising beta-  
485 emitters <sup>67</sup>Cu and <sup>47</sup>Sc. *J Radioanal Nucl Chem* 305:127–132 65.

486 Starovoitova VN, 2015b. <sup>47</sup>Ca production for <sup>47</sup>Ca/<sup>47</sup>Sc generator system using electron linacs. *Appl*  
487 *Radiat Isot* 97:188–192

488 Velikyan, I., 2012. Molecular imaging and radiotherapy: theranostics for personalized patient  
489 management. *Theranostics* 2(5), 424-426.

490 Yagi, M. and Kondo, K., 1977. Preparation of carrier-free <sup>47</sup>Sc by the <sup>48</sup>Ti(g,p) reaction. *Int. J. Appl.*  
491 *Radiat. Isot.* 28, 463-468.

492

493

494

495

496

497

498

499

500

501

502

503